nature photonics

ARTICLES

https://doi.org/10.1038/s41566-018-0190-8

Relativistic single-cycle tunable infrared pulses generated from a tailored plasma density structure

Zan Nie[1], Chih-Hao Pai[1*], Jianfei Hua[1], Chaojie Zhang[2], Yipeng Wu[1], Yang Wan[1], Fei Li[2], Jie Zhang[1], Zhi Cheng[1], Qianqian Su[1], Shuang Liu[1], Yue Ma[1], Xiaonan Ning[1], Yunxiao He[1], Wei Lu[1,3,4*], Hsu-Hsin Chu[5], Jyhpyng Wang[5,6,7], Warren B. Mori[2] and Chan Joshi[2]

The availability of intense, ultrashort coherent radiation sources in the infrared region of the spectrum is enabling the generation of attosecond X-ray pulses via high-harmonic generation, pump–probe experiments in the 'molecular fingerprint' region and opening up the area of relativistic infrared nonlinear optics of plasmas. These applications would benefit from multi-millijoule single-cycle pulses in the mid- to long-wavelength infrared region. Here, we present a new scheme capable of producing tunable relativistically intense, single-cycle infrared pulses from 5 to 14 μm with a 1.7% conversion efficiency based on a photon frequency downshifting scheme that uses a tailored plasma density structure. The carrier-envelope phase of the long-wavelength infrared pulse is locked to that of the drive laser to within a few per cent. Such a versatile tunable infrared source may meet the demands of many cutting-edge applications in strong-field physics and greatly promote their development.

The past decade has seen significant progress in the development of intense few-cycle mid-infrared (wavelength $\lambda < 5\,\mu m$) laser sources, which has opened new avenues in research on strong-field laser–matter interactions[1]. These mid-infrared sources are ideal tools for two-dimensional infrared spectroscopy[2], ultrafast X-ray highharmonic generation[3,4] and time-resolved imaging of molecular structures[5]. Furthermore, intense single-cycle mid-infrared pulses can inherently isolate the electron dynamics in strong-field interactions, which makes them very useful for investigating ultrafast phenomena in gases and solids. Some applications are coherent control of lattice displacements through nonlinear photonics[6], generation of isolated attosecond[7] or even zeptosecond X-ray pulses[8], and subfemtosecond control and metrology of bound-electron dynamics in atoms[9]. For many of these applications[4,8], a long carrier wavelength (~10 μm) is often preferred. However, generation of intense few-cycle long-wavelength infrared (LWIR) pulses is one of the current challenges to ultrafast laser technology. To date, the majority of high-intensity few-cycle mid-infrared sources rely on optical parametric amplifiers pumped by lasers operating at ~1 μm (refs [10,11]). However, these optical parametric amplifiers face significant challenges with an increase of wavelength beyond 5 μm due to a lack of nonlinear crystals with suitable optical and mechanical properties. Recently, there have been mid-infrared optical parametric chirped-pulse amplifier demonstrations with submillijoule energy and wavelength reaching beyond 5 μm in $ZnGeP_2$ crystals[12,13], pumped by high-energy, ~2 μm Ho-doped lasers[14–16], but the pulse duration is about 5–8 optical cycles. CO_2 lasers are important high-energy infrared sources in the 10 μm spectral range, but their wavelengths have limited tunability and their pulse durations are generally limited to a few picoseconds[17,18]. Some other methods, such as difference frequency generation[19], adiabatic difference frequency generation[20], non-degenerate four-wave-mixing[21–23] and optical rectification[24–26], have only attained microjoule-level pulse energy, which is not sufficient for strong-field applications. Apart from CO_2 lasers, the rest of the sources are 'indirect sources' of infrared radiation. There are also some post-processing methods, such as post compression[27,28] or synthesis[29], that are often more complex than the methods described above. In other words, the generation of coherent, ultra-intense infrared pulses is still an outstanding problem. Here we present an entirely different approach to solve this problem that utilizes asymmetric self-phase modulation (SPM) produced by a wake in a tailored (optimally shaped) plasma density structure such that the pump laser pulse continuously downshifts in frequency to give multi-millijoule energy, single-cycle LWIR radiation. Furthermore, the LWIR pulse is carrier-envelope phase (CEP) locked to the pump laser. The advantage of this scheme for infrared generation is that unlike in traditional nonlinear crystals, there is no damage limitation for the power/intensity scaling in plasmas, making it possible to generate relativistically intense single-cycle LWIR pulses.

Results

Photon frequency downconversion in a nonlinear plasma wake. It is well known that a portion of a short but intense laser pulse can be frequency downshifted rapidly as it excites a nonlinear wake (density disturbance) while propagating through a uniform underdense ($\omega_p < \omega_0$) plasma[30,31]. Here $\omega_p = (4\pi n_e e^2 / m_0)^{\frac{1}{2}}$ is the plasma frequency, n_e is the ambient plasma density, m_0 is the electron mass, e is the electron charge and ω_0 is the drive laser's carrier frequency. If the normalized vector potential $a_0 = eA / m_0c^2 > 2$ (A is the vector potential in Coulomb gauge and c is the speed of light in a vacuum), and the pulse duration $\tau < \sqrt{2\pi / \omega_p}$, the ponderomotive force (radiation pressure force) of the laser pulse eventually pushes out all the plasma electrons forward and outward, forming a three-dimensional (3D), nonlinear wake (a bubble-like

[1]Key Laboratory of Particle and Radiation Imaging of Ministry of Education, Department of Engineering Physics, Tsinghua University, Beijing, China. [2]University of California Los Angeles, Los Angeles, CA, USA. [3]State Key Laboratory of Low Dimensional Quantum Physics, Department of Physics, Tsinghua University, Beijing, China. [4]IFSA Collaborative Center, Shanghai Jiao Tong University, Shanghai, China. [5]Department of Physics, National Central University, Jhongli, Taiwan. [6]Institute of Atomic and Molecular Sciences, Academia Sinica, Taipei, Taiwan. [7]Department of Physics, National Taiwan University, Taipei, Taiwan. *e-mail: chpai@mail.tsinghua.edu.cn; weilu@mail.tsinghua.edu.cn

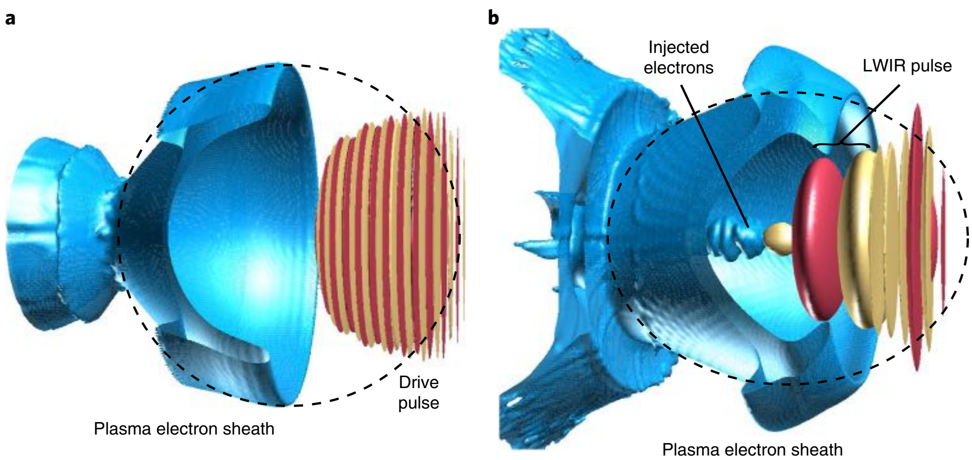

Fig. 1 | Illustration of photon frequency downconversion in a nonlinear plasma wake using a 3D particle-in-cell simulation showing cut-away views of wakes. a, At the beginning of the structure where the laser pulse has formed the spherical wake (dotted circle) but has not undergone substantial frequency modification. **b**, Near the end of the tailored density plasma structure where the laser pulse has been severely frequency downshifted and the LWIR pulse is seen to reside in the elongated (dotted ellipse) wake cavity. Some plasma electrons are injected into the wake and accelerated by it.

region containing mostly plasma ions encapsulated in a sheath of plasma electrons) as shown in Fig. 1a. If $a_0 > 1$, the plasma electrons oscillate relativistically (close to c) in the laser electric field. According to 1D nonlinear theory, the refractive index seen by the laser photons in the process varies as[32,33]: $\eta \simeq 1-\frac{\omega_p^2}{2\omega_0^2}\frac{1}{1+\phi}$, where Φ is the scalar potential in Coulomb gauge, $\phi = |e|\Phi / m_0c^2$ is the normalized scalar potential. It is the gradient of η (in the laser-rest frame: $\xi = z - ct$, where z is the longitudinal axis, and t is the time axis in laboratory frame) that leads to a decrease or an increase of the photon frequency. Specifically, photons in the front of the wake where $\partial\eta/\partial\xi$ is negative are frequency downshifted, while photons overlapping the tail of the wake where $\partial\eta/\partial\xi$ is positive are frequency upshifted, and the part in the central, near electron-free region experiences scarcely any frequency change. Therefore, the laser pulse undergoes frequency broadening due to SPM in the wake. This phenomenon has been well documented in the literature[30,34–37]. The first effort to utilize this technique for generating ultrashort mid-infrared pulses using a wake in a uniform plasma was reported in ref. [38], where about 1.5% of the 810 nm Ti:sapphire laser energy was converted into the 2–6 μm spectral range.

In the tailored plasma density structure that we propose here, the laser pulse is initially compressed—using a combination of SPM and group velocity dispersion (GVD) since $v_g \simeq c\left(1-\frac{\omega_p^2}{2\omega^2}\frac{1}{1+\phi}\right)$—and then rapidly further frequency downshifted in a higher-density plasma region to generate the LWIR photons. The LWIR photons then slip back to the central region of the wake due to dispersion/slower group velocity. The central region of the wake is devoid of plasma electrons ($\eta \sim 1$) and thus serves as a perfect container for the LWIR pulse (Fig. 1b). In this sense, the present method can be thought of as an optimized case of extremely asymmetric SPM aided by GVD within a plasma wake.

Efficient single-cycle infrared source using a tailored plasma density structure. As shown in Fig. 1, for photon frequency downconversion to dominate the laser pulse evolution, it must be short enough (typically <10 fs) so that the photons do work in pushing the plasma electrons outward. Such short pulses are often generated by pulse compression in hollow fibres[39], which can deliver ~10 mJ energy. To use such pulses to excite a nonlinear, fully blown-out wake, high-density (up to 10^{20} cm^{-3}) plasmas have to be used. However, in this case the LWIR pulse cannot be generated as its wavelength is longer than the plasma wavelength and the pulse undergoes both photon up- and downshifting as explained earlier. Here we put forward a general solution that uses commonly available longer laser pulses (for example, 30–50 fs from a Ti:sapphire laser) with high enough energy to excite a fully blown-out wake throughout the tailored plasma density structure. Our plasma structure consists of three different modules: the pulse compressor, the infrared converter and the output coupler as shown in Fig. 2a. First, the pulse compressor shortens the 30–50-fs-long pulse that then undergoes rapid frequency downconversion in the converter section. The final coupler section transports the infrared pulse out of the plasma efficiently while preserving its temporal quality.

We illustrate the physical processes occurring in each module of the plasma structure by showing the results obtained using the 3D particle-in-cell simulation code OSIRIS[40,41]. A laser pulse with an initial wavelength of 800 nm, a pulse energy of 1.2 J, a temporal full width at half maximum (FWHM) of the $\sin^2$ pulse of 30 fs and a spot size of 16 μm is propagated through the plasma structure. The initial a_0 is about 2.1. The density profile of the plasma structure, the FWHM pulse width and peak a_0 evolution, and the spectral evolution are shown in Fig. 2a–c, respectively.

From Fig. 2b, it can be seen that the laser pulse is compressed from 30 fs to about 11 fs in the compressor module and is further compressed to less than 4 fs in the transition region between the compressor and converter modules. Because of the relatively low plasma density and the longer laser pulse length (compared with that in the converter module), the spectrum of the pulse is only modestly broadened in the compressor module. Most of the frequency downconversion occurs in the higher-density converter module (Fig. 2c). The final coupler module simply transfers the pulse to outside with small attenuation and without any significant distortion due to GVD effects. The initial and final complete spectra of the pulse are shown in Fig. 2d. The LWIR portion appears as a distinct peak at the end of this spectrum (shaded region) and can be easily filtered. We find that this portion of the spectrum is nearly transform limited ($\Delta\nu\Delta\tau = 0.51$, where $\Delta\nu$ is the frequency bandwidth FWHM and $\Delta\tau$ is the pulse duration FWHM) and the oscillating field is only one period long as seen in the inset of Fig. 2d. The total conversion efficiency of the LWIR radiation in the range of 8–30 μm is about 1.7%. All these frequency components are phase locked to give a single-cycle pulse with a carrier wavelength of 12 μm.

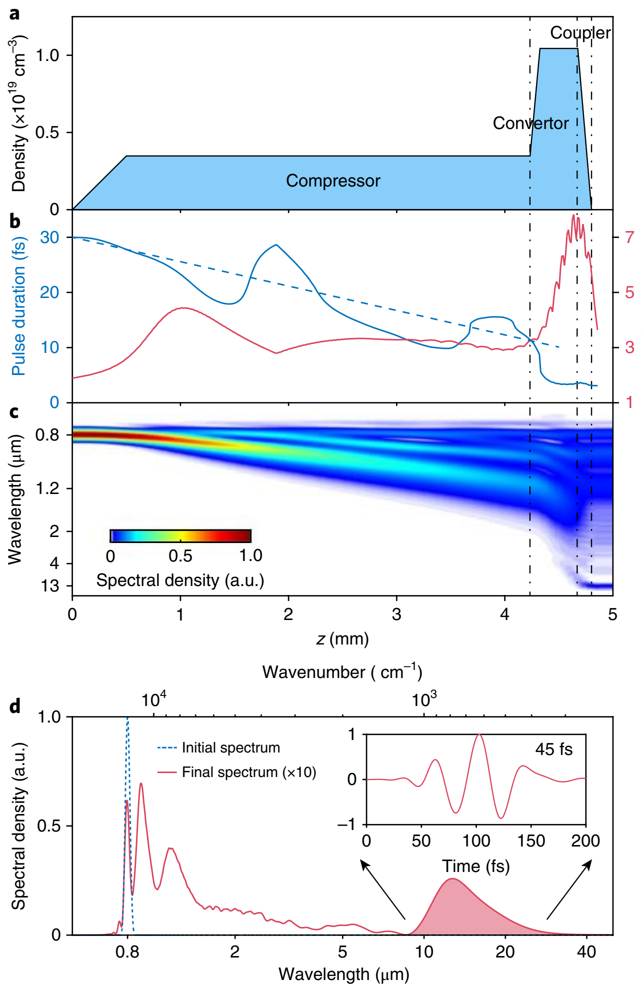

Fig. 2 | The structure and output of the LWIR source. a, The density profile of the plasma structure. **b**, The pulse duration and peak a_0 evolution with propagation distance in the plasma. The dotted blue line shows the general trend of the pulse duration variation in the compressor. **c**, The spectral evolution with the propagation distance in the plasma. **d**, The spectra of the laser pulse entering (blue dashed line) and exiting (red solid line) the plasma structure and the LWIR pulse (shaded region) that resides within the wake cavity shown in Fig. 1b. The inset shows the temporal variation of the electric field of the long-wavelength portion (shaded region) of the infrared pulse. The plasma length is about 5 mm or 5 Rayleigh lengths for the spot size we used. The wake encompasses much of the laser pulse and helps to guide it[42] over the entire length of the plasma structure.

In other words, about 20 mJ energy (0.44 TW) is contained in an approximately one wavelength cube volume leading to a relativistically intense pulse ($a_0 > 7$). The efficiency is ultimately limited by the pump to infrared frequency ratio (the quantum efficiency) and any attenuation of the infrared pulse due to the residual plasma. To the best of our knowledge, this conversion efficiency is among the highest of the 'indirect sources' in this spectral range.

Figure 3a–c shows the evolution of the wake in different modules, where y is the transverse axis that is perpendicular to the polarization direction of the electric field. Figure 3d–f shows the corresponding Wigner transforms (instantaneous wavenumber (frequency) as a function of time) of the on-axis electric field superimposed on the negative refractive index gradient ($-\partial\eta/\partial\xi$), where k is the wavenumber of the IR pulse and k_0 is the initial wavenumber of the drive pulse. As expected, when $\partial\eta/\partial\xi$ is negative (positive) the frequency is downshifted (upshifted) from the definition of instantaneous frequency as the rate of phase variation and thus the refractive index.

Now we discuss in detail the underlying physics in each module of the plasma structure. (1) Compressor module. In this module, the plasma density is relatively low (3.5×10^{18} cm^{-3}). The laser pulse creates a nonlinear wake as it enters the plasma. The varying refractive index gradient due to the wake formation causes the instantaneous frequency to vary locally along laser pulse. At the beginning of this module, the initially $\sin^2$ pulse occupies mostly the first half of the wake (Fig. 3a), so the whole laser pulse undergoes gentle frequency downshifting and develops a nearly linear chirp—because of an almost linear refractive index gradient (dashed-dotted line in Fig. 3d) over most of the pulse—which is optimal for self-compression by GVD. However, with the process of self-compression, the nearly linear refractive index gradient gradually becomes nonlinear (Fig. 3e). This leads to a higher-order chirp, and produces the variation of pulse duration (Fig. 2b). Overall, the negative GVD of the plasma results in self-compression of the laser pulse from 30 to 11 fs (Fig. 3b) so that the peak of the laser pulse is located where the refractive index gradient is the largest (Fig. 3e). This is the optimal duration for infrared generation in the converter module. (2) Converter module. The 1D nonlinear theory[32] can be used to design the laser and plasma parameters that are optimum for the converter module (see Methods). In this module, the plasma density is three times higher than that in the compressor. The converter length is only 450 µm including a 100 µm density up-ramp that serves as the transition region. The increase of plasma density leads to self-focusing and further self-compression of the drive pulse. This together with frequency downshifting of the photons leads to a rapid increase of a_0 of the pulse (from 2.1 to 7.8 as shown in Fig. 2b since $a_0 \propto E/\omega$, where E is the transverse electric field of the laser pulse). Throughout this module, the whole drive pulse resides in the very front of the wake where it experiences an extremely rapid change of the refractive index (Fig. 3c,f). The LWIR components slip rapidly backwards towards the centre of the wake due to their much slower group velocity. In this almost electron-free region of the wake, the LWIR pulse undergoes little further frequency change or dispersion. Meanwhile, the nonlinear wake wavelength is elongated ($\lambda_{\rm nl} = 2\pi c\sqrt{a_0} / \omega_{\rm p}$) due to an increase of a_0, which increases the volume of the ion cavity so that it can accommodate the LWIR pulse. At the end of this module, an intense ultrashort LWIR pulse with broad spectrum has been formed inside the wake cavity, with an extremely short near-infrared pulse at the leading front (Fig. 3c,f). (3) Coupler module. After the LWIR pulse is generated in the converter module, it has to be extracted from the plasma without either dispersive spreading or attenuation due to absorption. The closer the infrared frequency to the initial plasma frequency the worse is the attenuation. The coupler solves this problem by expanding the wake cavity size in the density down-ramp. This is so because the nonlinear wake wavelength (cavity size) is given by $\lambda_{\rm nl} \propto \sqrt{a_0} / \omega_{\rm p}$ and in the down-ramp a_0 (Fig. 2b) falls slower than $\omega_{\rm p}$. The programmable parameter here is the scale length $L = \left(\frac{1}{n_{\rm e}}\frac{{\rm d}n_{\rm e}}{{\rm d}z}\right)^{-1}$ of the falling plasma density $n_{\rm e}(z)$. The scale length of falling edge must be short enough so that the bubble expands quickly and the centre of the wake cavity retreats very quickly relative to the infrared pulse, so that the infrared pulse leaves the plasma with neither energy loss nor further frequency change. Otherwise, the centre of the wake still retreats relative to the infrared pulse but with a slower velocity. In this case, the infrared pulse can initially experience further frequency downconversion as it resides in the front of the wake again due to the retreat of the wake centre. However, the increase of the down-ramp length will lead to longer infrared pulse duration due to GVD. In Fig. 4a, we show how the central wavelength, the number of optical cycles and the conversion efficiency of the LWIR pulse are

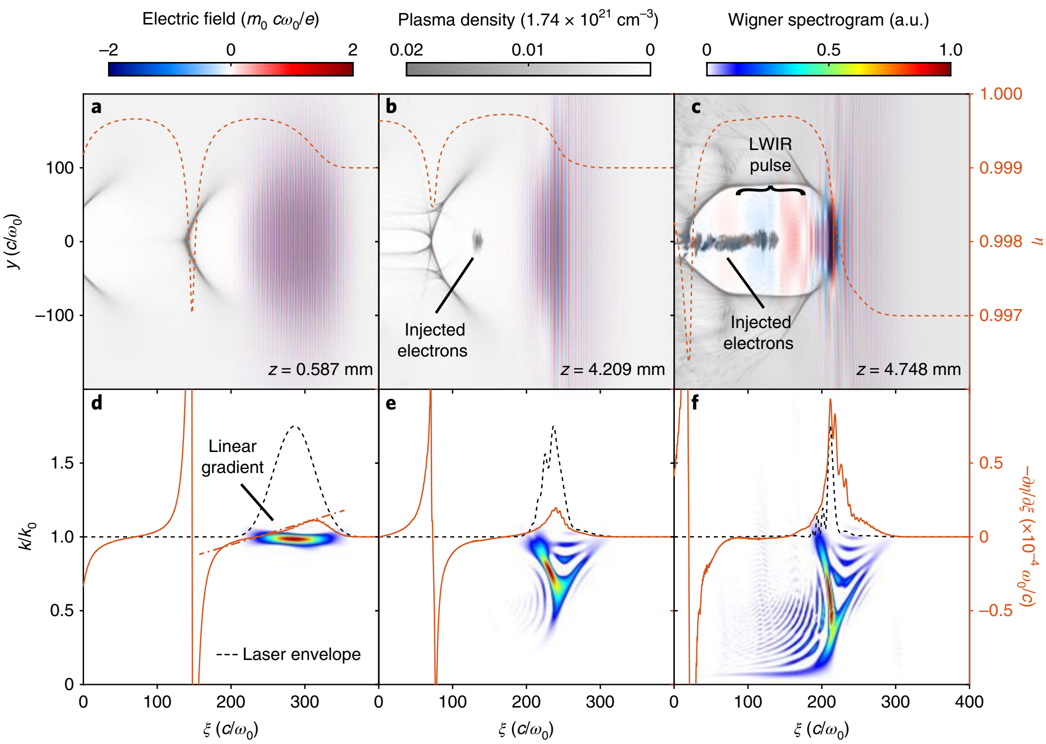

Fig. 3 | Photon frequency downconversion in a tailored plasma structure. **a**–**c**, The transverse electric field of the evolved laser pulse, the wake and on-axis refractive index (orange dashed line) are shown at the beginning of the uniform density part of the pulse compressor (**a**), at the end of the pulse compressor (**b**) and at the end of the infrared converter (**c**). **d**–**f**, The Wigner spectrograms of the on-axis transverse electric field, the refractive index gradient (orange solid line) and laser envelope (black dashed line) at the same position as in **a**–**c**, respectively. In **b** and **c**, the injection of some plasma electrons in the wake cavity is also seen.

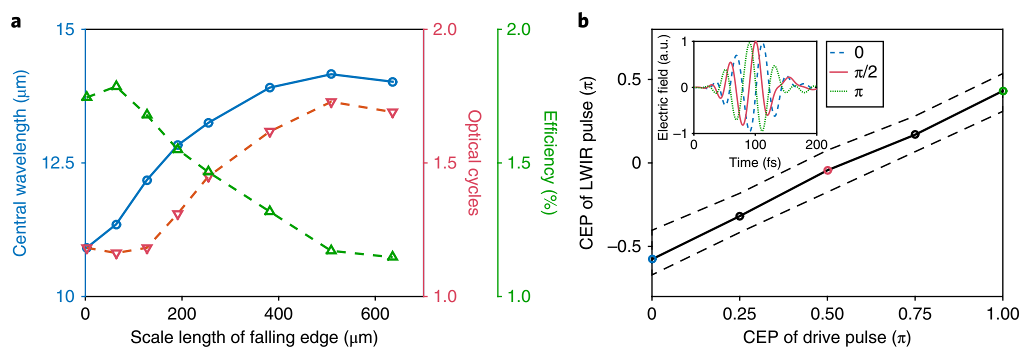

Fig. 4 | Parameter dependence of the LWIR pulse on the plasma falling edge scale length and the drive pulse CEP. **a**, Dependence of central wavelength, optical cycles and infrared conversion efficiency (8–30 μm) on the plasma falling edge scale length in the output coupler. **b**, The relationship between the CEP of the LWIR pulse and that of the initial drive pulse for the case shown in Fig. 2. The upper (lower) dashed black line is the result of increasing (decreasing) the integral of the plasma density and length by $3.3\times10^{19}\,\mathrm{cm^{-3}}\,\mu\mathrm{m}$. The inset shows the electric field of the filtered LWIR pulse for different initial CEP of the drive laser (blue dashed line, 0; red solid line, $\pi/2$; green dotted line, π).

affected by the scale length of the down-ramp of the coupler module for the case considered here. With the increase of the scale length of the falling edge, the central wavelength increases, the number of optical cycles also increases and the conversion efficiency drops. Taking all these factors into account, the optimal scale length of the falling edge for the example shown in Fig. 2 is about 130 μm.

CEP locking. We find that the CEP of the infrared pulse generated in this scheme is locked to the initial CEP of the drive pulse. This property will be especially desirable for multi-shot pump-probe applications.

When a transform-limited laser pulse propagates in plasma, the change in CEP is inevitable as the laser phase (carrier) velocity $v_p > c$ while its group (envelope) velocity $v_g < c$. The change in the phase of the electric field between the infrared pulse and the initial drive pulse measured at the peak intensity point of the two pulses is given by:

$$\Phi_{\mathrm{CEP}}-\Phi_0=\int_0^{l/c}\frac{2\pi(v_p-v_g)\,dt}{\lambda_{\mathrm{IR}}(t)}\approx\int_0^{l/c}\frac{n_e(t)}{n_c}\frac{\omega_0^2}{\omega_{\mathrm{IR}}(t)}\frac{dt}{1+\phi(t)} \quad (1)$$

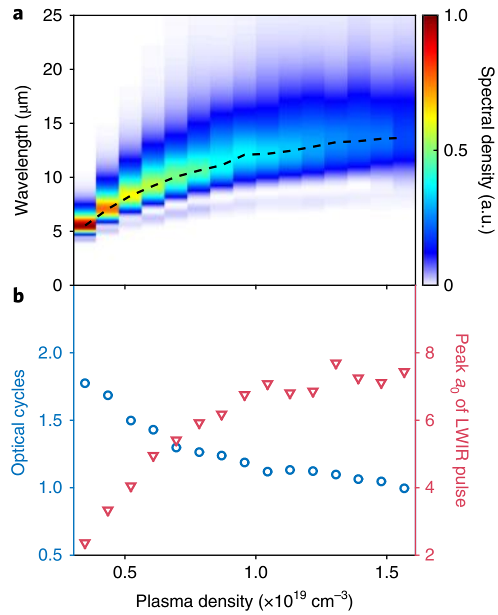

Fig. 5 | Effect of variation of plasma density on output parameters of the LWIR pulse in the converter module. a,b, Dependence of the infrared spectrum (**a**) and optical cycles and peak a_0 (**b**) on plasma density. The dashed line in **a** tracks the peak wavelength of the LWIR pulse.

where Φ_0 is the initial CEP of the drive pulse, ω_0 is the initial drive pulse frequency, $n_e(t)$ is the ambient plasma density, n_c is the critical plasma density for intial drive pulse, $\omega_{IR}(t)$ is the infrared pulse frequency and l is the total plasma length. Once the plasma density profile is fixed, the variation of the CEP caused by propagation is fixed. Then there is a linear mapping relationship between the CEP of the generated infrared pulse and that of the initial drive pulse. We use the same parameters used in Fig. 2 to illustrate this mapping. In Fig. 4b, we plot the CEP of the $\lambda = 12\,\mu m$ infrared pulse, as the CEP of the drive pulse is varied from 0 to π (for $\lambda = 0.8\,\mu m$) radians. The upper (lower) dashed black line in Fig. 4b shows the resulting CEP of the infrared pulse for the same drive pulse but with the plasma density–length product increased (decreased) by $3.3 \times 10^{19}\,cm^{-3}\,\mu m$. We can see that the two CEP phases track one another rather well in all three cases.

Based on equation (1), we can roughly estimate the CEP evolution at different sections. For the pulse compressor section, $\omega_{IR}(t)$ changes little due to gentle photon frequency downshifting (Fig. 2c), and $\phi(t)$ also changes little due to the small change of a_0 in this process (Fig. 2b). Therefore, the variation of the CEP is roughly dependent on the integral of the plasma density and length. For the infrared converter section, $\omega_{IR}(t)$ changes rapidly due to strong photon frequency downshifting (Fig. 2c), and $\phi(t)$ also changes rapidly due to rapid change of a_0 in this process (Fig. 2b). Interestingly, both these changes approximately compensate each other so that the variation of the CEP is still roughly dependent on the integral of the plasma density and length. For solid-state CEP-stable lasers, the CEP jitter is often less than 0.1π radians. As shown in Fig. 4b, to achieve the same degree of control, the jitter of the plasma density–length product should be less than $3.3 \times 10^{19}\,cm^{-3}\,\mu m$, as these two parameters are linearly correlated. Besides, while keeping the integral of the plasma density and length unchanged, we have changed the scale length of the up-ramp between the compressor and the converter in the range of 100–250 μm, and the CEP only changes by about 0.02π, which supports the physical explanation given above.

Discussion

We now discuss the robustness of this LWIR generation scheme in terms of the plasma parameters. We have found that not only are the density and length of the converter module the decisive factors for tuning the infrared central wavelength from 5 to 14 μm (Fig. 5a) but also that throughout the range of plasma densities considered here, the tunable infrared pulses are near single-cycle and relativistically intense (Fig. 5b). As stated earlier, the converter density is higher than the compressor density; however, the converter density cannot be made arbitrarily high because the pulse must reside in the portion of the wake where $\partial\eta/\partial\xi$ is negative. Furthermore, if the plasma density in the converter module is too high, the drive pulse may not be able to sustain a large enough cavity to contain the generated infrared pulse, resulting in significant attenuation. Besides, the scale length of the down-ramp must be shorter the higher the plasma density. This proves to be a practical limitation.

We point out that the plasma-accelerator community is already using similar tailored plasma density structures for the generation of high-brightness[43] beams and for overcoming dephasing between the accelerating electrons and the plasma wake[44]. Structured density modules with a density step ratio of 2–3 factors, peak densities on the order 1×10^{19}–$2 \times 10^{19}\,cm^{-3}$ and density ramps with scale lengths from 100–400 μm have already been demonstrated. We therefore believe that such tailored density structures will prove to be practical devices for generating tunable long-wavelength, intense, single-cycle pulses in the near future.

Methods

Methods, including statements of data availability and any associated accession codes and references, are available at https://doi.org/10.1038/s41566-018-0190-8.

Received: 14 December 2017; Accepted: 10 May 2018;
Published online: 11 June 2018

References

1. Wolter, B. et al. Strong-field physics with mid-IR fields. *Phys. Rev. X* **5**, 21034 (2015).
2. Calabrese, C., Stingel, A. M., Shen, L. & Petersen, P. B. Ultrafast continuum mid-infrared spectroscopy: probing the entire vibrational spectrum in a single laser shot with femtosecond time resolution. *Opt. Lett.* **37**, 2265–2267 (2012).
3. Popmintchev, T. et al. Bright coherent ultrahigh harmonics in the keV X-ray regime from mid-infrared femtosecond lasers. *Science* **336**, 1287–1291 (2012).
4. Weisshaupt, J. et al. High-brightness table-top hard X-ray source driven by sub-100-femtosecond mid-infrared pulses. *Nat. Photon.* **8**, 927–930 (2014).
5. Blaga, C. I. et al. Imaging ultrafast molecular dynamics with laser-induced electron diffraction. *Nature* **483**, 194–197 (2012).
6. Först, M. et al. Nonlinear phononics as an ultrafast route to lattice control. *Nat. Phys.* **7**, 854–856 (2011).
7. Silva, F., Teichmann, S. M., Cousin, S. L., Hemmer, M. & Biegert, J. Spatiotemporal isolation of attosecond soft X-ray pulses in the water window. *Nat. Commun.* **6**, 6611 (2015).
8. Hernández-García, C. et al. Zeptosecond high harmonic keV X-ray waveforms driven by midinfrared laser pulses. *Phys. Rev. Lett.* **111**, 033002 (2013).
9. Hassan, M. T. et al. Optical attosecond pulses and tracking the nonlinear response of bound electrons. *Nature* **530**, 66–70 (2016).
10. Andriukaitis, G. et al. 90 GW peak power few-cycle mid-infrared pulses from an optical parametric amplifier. *Opt. Lett.* **36**, 2755–2757 (2011).
11. Zhao, K. et al. Generation of 120 GW mid-infrared pulses from a widely tunable noncollinear optical parametric amplifier. *Opt. Lett.* **38**, 2159–2161 (2013).
12. von Grafenstein, L. et al. 5 μm few-cycle pulses with multi-gigawatt peak power at a 1 kHz repetition rate. *Opt. Lett.* **42**, 3796–3799 (2017).
13. Sanchez, D. et al. 7 μm, ultrafast, sub-millijoule-level mid-infrared optical parametric chirped pulse amplifier pumped at 2 μm. *Optica* **3**, 147–150 (2016).
14. von Grafenstein, L., Bock, M., Ueberschaer, D., Griebner, U. & Elsaesser, T. Picosecond 34 mJ pulses at kHz repetition rates from a Ho:YLF amplifier at 2 μm wavelength. *Opt. Express* **23**, 33142–33149 (2015).
15. von Grafenstein, L., Bock, M., Ueberschaer, D., Griebner, U. & Elsaesser, T. Ho:YLF chirped pulse amplification at kilohertz repetition rates—43 ps pulses at 2 μm with GW peak power. *Opt. Lett.* **41**, 4668–4671 (2016).
16. Malevich, P. et al. Broadband mid-infrared pulses from potassium titanyl arsenate/zinc germanium phosphate optical parametric amplifier pumped by Tm, Ho-fiber-seeded Ho:YAG chirped-pulse amplifier. *Opt. Lett.* **41**, 930–933 (2016).
17. Haberberger, D., Tochitsky, S. & Joshi, C. Fifteen terawatt picosecond CO_2 laser system. *Opt. Express* **18**, 17865–17875 (2010).

18. Polyanskiy, M. N., Pogorelsky, I. V. & Yakimenko, V. Picosecond pulse amplification in isotopic CO_2 active medium. *Opt. Express* **19**, 7717–7725 (2011).
19. Pupeza, I. et al. High-power sub-two-cycle mid-infrared pulses at 100 MHz repetition rate. *Nat. Photon.* **9**, 721–724 (2015).
20. Krogen, P. et al. Generation and multi-octave shaping of mid-infrared intense single-cycle pulses. *Nat. Photon.* **11**, 222–226 (2017).
21. Nomura, Y. et al. Phase-stable sub-cycle mid-infrared conical emission from filamentation in gases. *Opt. Express* **20**, 24741–24747 (2012).
22. Fuji, T., Nomura, Y. & Shirai, H. Generation and characterization of phase-stable sub-single-cycle pulses at 3000 cm^{-1}. *IEEE J. Sel. Top. Quantum Electron.* **21**, 8700612 (2015).
23. Pigeon, J. J., Tochitsky, S. Y., Welch, E. C. & Joshi, C. Measurements of the nonlinear refractive index of air, N_2, and O_2 at 10 μm using four-wave mixing. *Opt. Lett.* **41**, 3924–3927 (2016).
24. Junginger, F. et al. Single-cycle multiterahertz transients with peak fields above 10 MV/cm. *Opt. Lett.* **35**, 2645–2647 (2010).
25. Silva, F. et al. Multi-octave supercontinuum generation from mid-infrared filamentation in a bulk crystal. *Nat. Commun.* **3**, 807 (2012).
26. Pigeon, J. J., Tochitsky, S. Y., Gong, C. & Joshi, C. Supercontinuum generation from 2 to 20 μm in GaAs pumped by picosecond CO_2 laser pulses. *Opt. Lett.* **39**, 3246–3249 (2014).
27. Mitrofanov, A. V. et al. Subterawatt few-cycle mid-infrared pulses from a single filament. *Optica* **3**, 299–302 (2016).
28. Shumakova, V. et al. Multi-millijoule few-cycle mid-infrared pulses through nonlinear self-compression in bulk. *Nat. Commun.* **7**, 12877 (2016).
29. Liang, H. et al. High-energy mid-infrared sub-cycle pulse synthesis from a parametric amplifier. *Nat. Commun.* **8**, 141 (2017).
30. Gordon, D. F. et al. Asymmetric self-phase modulation and compression of short laser pulses in plasma channels. *Phys. Rev. Lett.* **90**, 215001 (2003).
31. Tsung, F. S., Ren, C., Silva, L. O., Mori, W. B. & Katsouleas, T. Generation of ultra-intense single-cycle laser pulses by using photon deceleration. *Proc. Natl Acad. Sci. USA* **99**, 29–32 (2002).
32. Sprangle, P., Esarey, E. & Ting, A. Nonlinear theory of intense laser–plasma interactions. *Phys. Rev. Lett.* **64**, 2011–2014 (1990).
33. Sprangle, P., Esarey, E. & Ting, A. Nonlinear interaction of intense laser pulses in plasmas. *Phys. Rev. A* **41**, 4463–4469 (1990).
34. Wilks, S. C., Dawson, J. M., Mori, W. B., Katsouleas, T. & Jones, M. E. Photon accelerator. *Phys. Rev. Lett.* **62**, 2600–2603 (1989).
35. Esarey, E., Ting, A. & Sprangle, P. Frequency shifts induced in laser pulses by plasma waves. *Phys. Rev. A* **42**, 3526–3531 (1990).
36. Mori, W. B. The physics of the nonlinear optics of plasmas at relativistic intensities for short-pulse lasers. *IEEE J. Quantum Electron.* **33**, 1942–1953 (1997).
37. Zhu, W., Palastro, J. P. & Antonsen, T. M. Pulsed mid-infrared radiation from spectral broadening in laser wakefield simulations. *Phys. Plasmas* **20**, 073103 (2013).
38. Pai, C.-H. et al. Generation of intense ultrashort midinfrared pulses by laser–plasma interaction in the bubble regime. *Phys. Rev. A* **82**, 063804 (2010).
39. Guénot, D. et al. Relativistic electron beams driven by kHz single-cycle light pulses. *Nat. Photon.* **11**, 293–296 (2017).
40. Fonseca, R. A. et al. OSIRIS: a three-dimensional, fully relativistic particle in cell code for modeling plasma based accelerators. In *Computational Science — ICCS 2002* (eds Sloot, P. M. A., Tan, C. J. K., Dongarra, J. J. & Hoekstra, A. G.) 342–351 (Lecture Notes in Computer Science Vol. 2331, Springer, Berlin, Heidelberg, 2002).
41. Fonseca, R. A. et al. One-to-one direct modeling of experiments and astrophysical scenarios: pushing the envelope on kinetic plasma simulations. *Plasma Phys. Control. Fusion* **50**, 124034 (2008).
42. Ralph, J. E. et al. Self-guiding of ultrashort, relativistically intense laser pulses through underdense plasmas in the blowout regime. *Phys. Rev. Lett.* **102**, 175003 (2009).
43. Xu, X. L. et al. High quality electron bunch generation using a longitudinal density-tailored plasma-based accelerator in the three-dimensional blowout regime. *Phys. Rev. Accel. Beams* **20**, 111303 (2017).
44. Guillaume, E. et al. Electron rephasing in a laser-wakefield accelerator. *Phys. Rev. Lett.* **115**, 155002 (2015).

Acknowledgements

This work was supported by the National Natural Science Foundation of China (NSFC) Grants No. 11425521, No. 11535006, No. 11475101 and No. 11775125, the National Basic Research Program of China No. 2013CBA01501, the Thousand Young Talents Program, the Air Force Office of Scientific Research (AFOSR) under award number FA9550-16-1-0139 DEF, the Office of Naval Research (ONR) Multidisciplinary University Research Initiative (MURI) (4-442521-JC-22891), the US Department of Energy grant DE-SC001006 and the Ministry of Science and Technology of Taiwan under Grant No. MOST-105-2112-M-001-005-M3. The simulations were performed on Sunway TaihuLight.

Author contributions

Z.N., C.-H.P. and W.L. proposed the concept. Z.N. developed the theoretical model and carried out the simulations. Z.N., C.J., W.L. and C.-H.P. wrote the paper. All authors contributed extensively to the work presented in this paper.

Competing interests

The authors declare no competing interests.

Additional information

Supplementary information is available for this paper at https://doi.org/10.1038/s41566-018-0190-8.

Reprints and permissions information is available at www.nature.com/reprints.

Correspondence and requests for materials should be addressed to C.-H.P. or W.L.

Methods

Theoretical estimate of the optimal pulse duration and plasma length of the infrared converter. We use 1D quasi-static nonlinear theory[32] to estimate the optimal pulse duration and the length of the infrared converter. The evolution of the vector potential of the laser pulse and the scalar potential of the wake are given by the following coupled equations[32]:

$$\left[-\frac{2}{c}\frac{\partial}{\partial\xi}-\frac{1}{c^2}\frac{\partial}{\partial\tau}\right]\frac{\partial\mathbf{a}}{\partial\tau}=k_p^2\frac{\mathbf{a}}{1+\phi} \quad (2)$$

$$\frac{\partial^2\phi}{\partial\xi^2}=\frac{k_p^2}{2}\left[\frac{1+a^2}{(1+\phi)^2}-1\right] \quad (3)$$

where $\xi=ct-z$, $\tau=t$ are the speed of light coordinates and $\phi=|e|\Phi/m_0c^2$ is the normalized scalar potential. When $|\phi|\ll 1$, it can be expressed as[33]:

$$\phi\approx\frac{k_p}{2}\int_{\xi}^{0}a_L^2(\xi')\sin[k_p(\xi'-\xi)]\,\mathrm{d}\xi' \quad (4)$$

where a_L is the envelope amplitude of the normalized vector potential $\mathbf{a}$, $k_p=\frac{\omega_p}{c}$, $\omega_p=\left(\frac{4\pi|e|^2n_e}{m_0}\right)^{\frac{1}{2}}$ is the ambient plasma frequency and n_e is the ambient plasma density. If the pulse envelope is given by $a_L=a_0\sin^2(\pi\xi/L)$ for $-L\le\xi\le 0$ (here $t=-L$ and $t=0$ are the time boundaries of the pulse), we obtain:

$$\phi\approx\left(\frac{p}{16}\right)^2\{12\theta^2-[1-\cos(2\theta)][7-\cos(2\theta)]\} \quad (5)$$

where $p=k_pa_0L/\pi$ and $\theta=\pi\xi/L$. The local wavenumber of the laser pulse is modified during the interaction with the plasma due to the refractive index gradient, which can be expressed by φ in 1D theory. Then the photon frequency downshifting rate is expressed as[36]:

$$\begin{aligned}r&\equiv\frac{1}{k}\frac{\partial k}{\partial(c\tau)}\\&\approx-\frac{1}{2}\frac{k_p^2}{k^2}\frac{1}{(1+\phi)^2}\frac{\partial\phi}{\partial\xi}=-\frac{\pi}{2L}\frac{k_p^2}{k^2}\frac{1}{(1+\phi)^2}\frac{\partial\phi}{\partial\theta}\end{aligned} \quad (6)$$

Inserting equation (5) into equation (6), we obtain the photon frequency downshifting rate. From equation (5) and (6), we know that for a given parameter p, the profile of the photon frequency downshifting rate is determined and accordingly the position of the maximum photon frequency downshifting rate θ_m (extreme point) is determined. Then there is a certain relationship between them, which is shown in the Supplementary Information.

When $\theta_m=\pi/2$, the position of the maximum photon frequency downshifting rate overlaps with the peak of the laser pulse. Numerically, we find that the optimal p is 2.88, which agrees very well with simulation results. Then for given plasma density and normalized vector potential of drive pulse, the optimal drive pulse length can be obtained:

$$L\approx\frac{1.44\lambda_p}{a_0} \quad (7)$$

where λ_p is the plasma wavelength. Here, $a_0\gg 1$ should be satisfied to make sure that the premise of the derivation ($L\ll\lambda_p$) is still valid. To get a comparable parameter with experiments, the pulse duration (FWHM of intensity) is given by:

$$c\tau\approx 0.36L\approx\frac{0.52\lambda_p}{a_0} \quad (8)$$

Inserting $\theta_m=\pi/2$ into equation (5) and equation (6), the maximum photon frequency downshifting rate r_m is obtained (assuming the optimal pulse duration):

$$r_m\approx-0.1\frac{k_p^3}{k^2}a_0 \quad (9)$$

If $a_0=$constant, the wavenumber of the IR pulse can be written as:

$$k^2\approx k_0^2-0.2k_p^3a_0l \quad (10)$$

where k_0 is the initial wavenumber and l is the propagation distance in plasma. In the case of large frequency downshifting, $k\ll k_0$, then we can obtain the optimal plasma length l_m to obtain the LWIR pulse:

$$l_m\approx\frac{5k_0^2}{k_p^3}a_0^{-1} \quad (11)$$

In practice, the whole pulse cannot undergo photon frequency downshifting with the maximum rate, and therefore the plasma length should be increased by up to a factor of 2. In addition, a_0 changes a lot due to strong self-focusing and self-compression in high-density plasmas. Therefore, a_0 is an average value over time in equation (11).

Particle-in-cell simulations. The 3D particle-in-cell simulations were carried out using the code OSIRIS[40,41] in Cartesian coordinates with a window moving at the speed of light. The z axis was defined to be the drive laser propagating direction. The simulation window had dimensions of $102\times102\times61$ μm with $600\times600\times2{,}400$ cells in the x, y and z directions, respectively. This corresponded to cell sizes of $\Delta x=\Delta y=1.33k_0^{-1}$ and $\Delta z=0.2k_0^{-1}$ (where $k_0=2\pi\lambda_0^{-1}$ is the drive laser wavevector and $\lambda_0=800$ nm). The number of macro-electrons per cell was 2.

The parameter scan was carried out using the quasi-3D OSIRIS[45,46] to save simulation time. Simulations were performed using a mesh with $\Delta r=k_0^{-1}$ and $\Delta z=0.2k_0^{-1}$ and the first two Fourier modes. The number of macro-electrons per cell was 4.

Data availability. The data that support the plots within this paper and other findings of this study are available from the corresponding authors upon reasonable request.

References

45. Lifschitz, A. F. et al. Particle-in-cell modelling of laser–plasma interaction using Fourier decomposition. *J. Comput. Phys.* **228**, 1803–1814 (2009).
46. Davidson, A. et al. Implementation of a hybrid particle code with a PIC description in r–z and a gridless description in ϕ into OSIRIS. *J. Comput. Phys.* **281**, 1063–1077 (2015).